Acta Crystallographica Section A
Foundations of Crystallography
ISSN 0108-7673

Received 5 November 2010
Accepted 15 February 2011

Simultaneous determination of highly precise Debye–Waller factors and multiple structure factors for chemically ordered tetragonal FePd

Xiahan Sang,* Andreas Kulovits and Jorg Wiezorek

Department of Materials Science and Mechanical Engineering, Swanson School of Engineering, University of Pittsburgh, 648 Benedum Hall, Pittsburgh, PA 15261, USA. Correspondence e-mail: xis20@pitt.edu

Accurate Debye–Waller (DW) factors and low-index structure factors up to 222 of chemically ordered FePd have been measured at 120 K. Ordered FePd has a simple tetragonal unit cell (*tP*2, *P*4/*mmm*) with Fe and Pd atoms at 0, 0, 0 and at $\frac{1}{2}, \frac{1}{2}, \frac{1}{2}$, respectively, requiring the measurement of four different DW factors. It was possible to simultaneously determine all four DW factors and several low-order structure factors using different, special off-zone-axis multi-beam convergent-beam electron diffraction patterns with high precision and accuracy. The different diffraction conditions exhibit different levels of sensitivity to changes in DW and structure factors. Here the sensitivity of different off-zone-axis convergent-beam electron diffraction patterns with respect to changes in DW factors and structure factors is discussed.

1. Introduction

Quantitative convergent-beam electron diffraction (QCBED or CBED) has been widely used to measure highly precise structure factors of oxides to evaluate the nature of interatomic bonds in these materials (Friis *et al.*, 2004; Zuo *et al.*, 1999; Ogata *et al.*, 2004; Jiang *et al.*, 2003; Streltsov *et al.*, 2001; Zuo *et al.*, 1997). The large magnitude of charge transfer and pronounced localization in ionic structures compared to covalently and metallically bonded materials lead to larger differences between experimentally determined structure factors and those obtained from the independent-atom model (IAM) approximations. In pure elemental metals and intermetallic alloys, especially those involving only transition metals, these differences are much smaller, owing to a rather delocalized electronic charge distribution. As a result, the precision and accuracy of CBED measurements and refinements for pure elemental metals and most intermetallics have to be much higher compared to the case of ionic structures. A few metals such as Cu (*A*1, *cF*4, $Fm\bar{3}m$) (Jiang *et al.*, 2004; Friis *et al.*, 2005) and some intermetallics which contain at least one atom species that is not a transition metal, *e.g.* transition-metal aluminides such as cubic *B*2-ordered NiAl (*B*2, *cP*2, $Pm\bar{3}m$) (Nüchter *et al.*, 1998*b*), cubic $L1_2$-ordered Ni_3Al ($L1_2$ or Cu_3Au structure, *cP*4, $Pm\bar{3}m$) (Zhu *et al.*, 1997) and tetragonal $L1_0$-ordered TiAl ($L1_0$ or CuAu-I structure, *tP*2, *P*4/*mmm*) (Holmestad & Birkeland, 1998), were investigated regarding electron-density distribution and bonding by CBED with some success. Investigations of metallic systems with non-cubic crystal structures which only contain heavier transition metals have not been pursued successfully to date. The paucity of experimental CBED studies for electron-density determination for transition metals and the chemically ordered compounds based on them can be attributed to the required high precision and accuracy in the experimental measurements, resulting from the fact that only a very small fraction of the large number of total electrons in the unit cells are bonding contributing electrons. In this study we use a recently introduced highly accurate experimental CBED technique (Sang *et al.*, 2010*a*) to investigate experimentally the electron-density determination for simple tetragonal, chemically ordered and ferromagnetic $L1_0$-phase FePd.

$L1_0$-ordered FePd, the γ_1 phase in the binary Fe–Pd system, is a layered structure with a *tP*2 unit cell ($L1_0$, *tP*2, *P*4/*mmm*) with an Fe atom at 0, 0, 0 and a Pd atom at $\frac{1}{2}, \frac{1}{2}, \frac{1}{2}$, and lattice parameters $a = 2.722$ and $c = 3.714$ Å (Ichitsubo & Tanaka, 2004). Conventionally, a larger unit cell with lattice constants $a' = 3.849$ and $c' = 3.714$ Å is used for convenience, which is based on a *tP*4 unit cell with two Fe atoms at 0, 0, 0 and $\frac{1}{2}, \frac{1}{2}, 0$, and two Pd atoms at $\frac{1}{2}, 0, \frac{1}{2}$ and $0, \frac{1}{2}, \frac{1}{2}$, respectively. The larger conventional *tP*4 unit cell more clearly illustrates the relationship between the chemically ordered $L1_0$ phase and the high-temperature face-centered cubic (f.c.c.) (*A*1, *cF*4, $Fm\bar{3}m$) phase from which it derives.

$L1_0$ FePd is a strong ferromagnetic intermetallic phase which, depending on the orientation of the crystalline lattice with respect to the incident beam, can lead to large distortions in experimental CBED patterns, thereby complicating the refinement for structure-factor measurements. Additionally, owing to the tetragonal symmetry of the $L1_0$ structure of the

γ_1-phase FePd, anisotropic Debye–Waller (DW) factors have to be introduced for each of the transition-metal elements. The magnitudes of the DW factors for each atom species differ along the crystallographically distinct [100] and [001] directions. Hence, four (two for each atom species) rather than two DW factors are required to describe this binary tetragonal phase. The accurate measurement of those four DW factors is essential for the determination of X-ray structure factors and the charge distributions (Saunders *et al.*, 1995; Sang *et al.*, 2010*b*). The values of the DW factors for the Fe and Pd atoms in the chemically ordered γ_1-phase FePd are predicted to differ significantly from those known for these atoms in the respective elemental transition metals in their stable crystalline structures at a given temperature because of effects from intermetallic bonding. For instance, the Al and Ni atoms in the respective elemental crystals of an f.c.c. structure are known to have room-temperature DW factors of B(Al) = 0.86 (1) and B(Ni) = 0.37 (1) Å^2 (Butt *et al.*, 1988), while in the $B2$-ordered NiAl the respective DW factors are B(Al) = 0.47 (1) and B(Ni) = 0.51 (1) Å^2 (Georgopoulos & Cohen, 1977). Using the DW factor values known for the elemental crystals, *e.g.* at room temperature for Fe B(Fe) = 0.35 Å^2 and for Pd B(Pd) = 0.45 Å^2 (Butt *et al.*, 1988), as starting values may introduce significant uncertainty in computational refinements for structure-factor determination. As only a few percent (∼1–3%) of the total electron charge distribution made up of 72 electrons (Fe^{26}, Pd^{46}) present in $L1_0$-ordered FePd are expected to contribute to the intermetallic bond, the errors of the measurement after refinement have to be less than 0.1% for structure factors to yield meaningful electron charge distributions. In this study we show that the highly precise and accurate CBED method, introduced by Sang *et al.* (2010*c*) and successfully applied previously to another chemically ordered intermetallic system NiAl, allowed us to measure and refine simultaneously structure and DW factors for the $L1_0$-ordered FePd system.

We used a newly adapted QCBED method to obtain simultaneously highly accurate and precise DW factors and multiple structure factors from CBED experiments utilizing off-zone-axis multi-beam orientations. This method involves selection of sample–beam orientations that are sensitive to both DW factors and structure factors. By tilting the sample systematically away from a zone axis by less than 1°, three or five diffracted beams are forced to intersect the Ewald sphere and fulfil the Bragg condition exactly. Those diffracted beams are then strongly excited and the dynamical interactions between diffracted beams with each other and the transmitted beam ensure high sensitivity of the intensity distribution in CBED patterns with changes in DW and structure factors. In this study we applied this method to a non-cubic system, namely, the strongly and uniaxially ferromagnetic FePd intermetallic phase with a chemically ordered tetragonal $L1_0$ structure, and we were able to obtain complete sets of DW and large sets of both electron and X-ray structure factors with unprecedented accuracy and precision that can be used for electron charge-density distribution determination.

2. Experiments

2.1. Sample preparation

$L1_0$ FePd samples used for TEM (transmission electron microscopy) investigations were prepared from an equiatomic chemically disordered f.c.c. γ-FePd ($A1$, $cF4$, $Fm\bar{3}m$) single crystal. This f.c.c. single crystal had been grown by the Bridgeman method and details of the crystal preparation have been reported by Al-Ghaferi *et al.* (2006). Sections were cut such that single-crystalline TEM samples with surface plane normal axes parallel to [001] and [110] directions could be fabricated. The plates were first heat treated at 823 K for 5 h to fully order the specimens. Subsequently, a heat treatment for 95 h at 873 K was carried out to maximize the grain size. Finally, to maximize the long-range-order (LRO) parameter and reduce the point-defect concentration the samples were heat treated at 673 K for 24 h. From the ordered plates 3 mm discs were obtained, which were mechanically thinned to a final thickness of about ∼50 µm prior to electro-polishing. The 3 mm discs were then electro-polished with a Struers TenuPol-5 twin-jet polishing unit using a solution of 82% acetic acid, 9% perchloric acid and 9% ethanol at 279 K. Prior to each TEM session the electro-polished $L1_0$ FePd TEM samples were plasma-cleaned using a South Bay Technology 'PC 2000' Plasma Cleaner to remove carbonaceous contamination from the sample surface.

2.2. Experimental CBED and data pre-processing

Experimental CBED patterns were acquired using a Jeol JEM 2100 F transmission electron microscope operated at nominally 200 kV and equipped with a GIF TRIDIEM post-column energy filter (Gatan Inc.). A low-background, double-tilt cooling stage holder (Gatan Inc.) was used to acquire CBED patterns at temperatures as low as liquid-nitrogen temperature to reduce thermal diffuse scattering (TDS). As temperatures above the minimum temperature, liquid-N_2 temperature ∼100 K, can be stabilized very well for extended periods using a smart temperature controller integrated in the cold stage, we obtained our CBED patterns at 120 K. Zero-loss peak energy-filtered CBED patterns were acquired with a 5–8 eV-wide energy-selecting slit. An electron-beam diameter of 0.5 nm was used in order to eliminate thickness variations in the illuminated area that could give rise to intensity variations in the CBED pattern intensity. The CBED patterns were recorded on a charge-coupled device (CCD) camera with a maximum resolution of 2048 × 2048.

The accelerating voltage was measured as ∼203 kV (3 kV offset due to the GIF TRIDIEM post-column energy filter) using the intersecting HOLZ (higher-order Laue zone) method with a silicon sample (Zuo, 1992). Incident-beam–sample orientations were determined using disc features and the symmetry thereof (Buxton *et al.*, 1976). Discs with excitation errors $\mathbf{s}$ close or equal to zero were selected for refinement, since the signal-to-noise ratio in those discs is advantageous. Each point in the selected discs is associated with a beam direction, which is used to calculate a theoretical intensity based on Bloch-wave methods (Bethe, 1928; Spence,

1993; Tsuda & Tanaka, 1995; Sang *et al.*, 2010*b*). The experimental intensity of each point is directly extracted from the image file. As the background signal around the discs is negligible (about 0.5% of the peak intensity in energy-filtered QCBED patterns), *i.e.* inelastic scattering is minimal at the measuring temperature of ~120 K, the background inside the discs is set to zero. As peak positions are more important than the intensity of peaks (Nakashima & Muddle, 2010), it is reasonable to ignore background. Each disc contains at least 80 000 data points, which is sufficient for accurate refinements.

2.3. Refinement procedure

During refinements intensity distributions of experimental CBED patterns are compared with simulated CBED patterns. Intensity distributions in simulated patterns are calculated based on Bloch-wave theory, which has been described previously (Bethe, 1928; Spence, 1993). The goal of the refinement is to minimize the objective function S, which measures the difference between the observed experimental intensity, $I_i^{\rm obs}$, and the calculated intensity, $I_i^{\rm cal}$, and is defined as

$$S = \sum_i (I_i^{\rm obs} - cI_i^{\rm cal})^2, \tag{1}$$

with c as the scaling factor. The optimization is realized by variation of electron structure factors U_g, sample thickness, sample orientation, accelerating voltage *etc.* During the refinement several low-order electron structure factors U_g with $h^2 + k^2 + l^2 < 12$ are relaxed, as only low-order hkl planes are affected strongly by bonding. High-order electron structure factors are approximated using the IAM approximation. IAM values for higher-order electron structure factors $U_g^{\rm higher\ order}$ $(h^2 + k^2 + l^2 > 12)$ are obtained by application of the Mott formula using IAM X-ray atomic scattering factors

$$U_g^{\rm higher\ order} = \frac{\gamma}{C\Omega s^2} \times \left[\sum_i (Z_i - f_i^{\rm XRD}) \exp(-B_i s^2) \exp(-2\pi i \mathbf{g}\mathbf{r}_i)\right] \tag{2}$$

in general, or for $L1_0$-ordered γ_1-FePd using the $tP2$ cell with Fe at (0, 0, 0) and Pd at $(\frac{1}{2}, \frac{1}{2}, \frac{1}{2})$

$$U_g^{\rm higher\ order} = \frac{\gamma}{C\Omega s^2}\Big[(Z_{\rm Fe} - f_{\rm Fe}^{\rm XRD}) \exp(-B_{\rm Fe} s^2) + (Z_{\rm Pd} - f_{\rm Pd}^{\rm XRD})(-1)^{h+k+l} \exp(-B_{\rm Pd} s^2)\Big] \tag{3}$$

with $s = g_{hkl}/2$, Ω = volume of the unit cell, γ = relativistic constant, $C = 131.2625$ if Å are used as a unit, $Z_i = Z_{\rm Fe}$ and $Z_{\rm Pd}$, the atomic numbers for Fe (26) and Pd (46), respectively (Spence & Zuo, 1992), $f_i^{\rm XRD}$ = X-ray atomic scattering factors $f_{\rm Fe}^{\rm XRD}$ and $f_{\rm Pd}^{\rm XRD}$ for Fe and Pd, respectively, and B_i = Debye–Waller factors $B_{\rm Fe}$ and $B_{\rm Pd}$ for Fe and Pd in the $L1_0$-ordered γ_1-FePd. In this formulation the DW factors can be interpreted as dampening terms.

While in this approximation for $U_g^{\rm higher\ order}$ the X-ray atomic scattering factors are fixed and approximated with readily available IAM values (Doyle & Turner, 1968), the DW factors B_i are relaxed. Using this formalism allows us to integrate DW factors into our routine and refine them simultaneously with low-order electron structure factors U_g. In total three to ten low-order $U_g (h^2 + k^2 + l^2 < 12)$ electron structure factors and the DW factors are relaxed simultaneously.

In order to ensure that a global rather than a local minimum is reached we provide reasonable starting values for the low-order electron structure factors and for the DW factors. Reasonable starting values for the DW factors are obtained from refinements with fixed electron structure factors, which are approximated with IAM values obtained from equation (3).

Using these newly obtained starting values for DW factors and IAM values for low- and high-order structure factors, the set of low-order electron structure factors and DW factors are refined simultaneously in a subsequent refinement run. Low-order electron structure factors are then subsequently converted into X-ray structure factors using

$$F_g^{\rm X} = Z_{\rm Fe} \exp[-B({\rm Fe}) s^2] + (-1)^{h+k+l} Z_{\rm Pd} \exp[-B({\rm Pd}) s^2] - \left(\frac{C\Omega s^2}{\gamma}\right) U_g. \tag{4}$$

The successful refinement of low-order electron structure and DW factors from a CBED pattern depends not only on the sensitivity of the intensity distribution in the pattern to the changes in low-order but also on the sensitivity to changes of high-order electron structure factors, as they are used to refine DW factors. Refinement of DW factors alone could lead to systematic errors (Saunders *et al.*, 1999).

Absorption factors are calculated with a method described by Bird & King (1990) and treated in a similar way to electron structure factors. Low-order absorption factors are relaxed independently during the refinement. High-order absorption factors are varied indirectly in the refinement as DW factors are optimized. The goodness of fit (GOF) is evaluated using a weighted reliability factor (Tsuda & Tanaka, 1995),

$$R_{\rm W} = \left[\frac{\sum_i (I_i^{\rm obs} - cI_i^{\rm cal})^2/\sigma_i^2}{\sum_i (I_i^{\rm obs})^2/\sigma_i^2}\right]^2, \tag{5}$$

with the standard deviation for the ith point. Generally, $\sigma_i = (I_i^{\rm obs})^{1/2}$. A smaller $R_{\rm W}$ can be interpreted as a better correspondence of the observed with theoretically determined intensities, *i.e.* a smaller $R_{\rm W}$ corresponds to a better refinement. The perfect fit between the observed and the calculated CBED patterns would result in an $R_{\rm W}$ value that is zero, *i.e.* when $I_i^{\rm obs}$ is identical to $cI_i^{\rm cal}$.

3. Results

3.1. Anisotropic DW factors

In the $tP2$ description of the $L1_0$-ordered γ_1-phase FePd, Fe and Pd atoms are at 0, 0, 0 (Wyckoff site a) and $\frac{1}{2}, \frac{1}{2}, \frac{1}{2}$

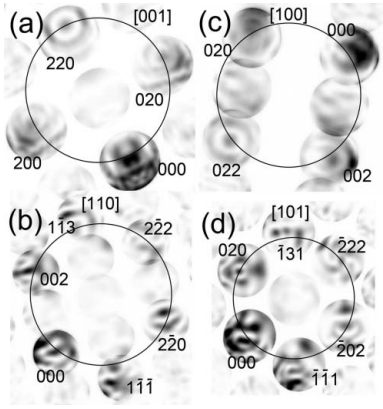

Figure 1
Off-zone-axis multi-beam condition patterns acquired near (*a*) [001], (*b*) [110], (*c*) [100] and (*d*) [101] orientations. The circle in each pattern represents the trace of Ewald sphere intersecting the zone-order plane in reciprocal space.

(Wyckoff site *d*), respectively. Owing to the symmetry of the tetragonal unit cell, atoms on both Wyckoff sites have two different non-zero DW factors ($B_{11} = B_{22}$, B_{33}, $B_{12} = B_{13} = B_{23} = 0$) (Willis & Pryor, 1975). Therefore, four different DW factors [$B(\mathrm{Fe})_{11}$, $B(\mathrm{Pd})_{11}$, $B(\mathrm{Fe})_{33}$ and $B(\mathrm{Pd})_{33}$] have to be measured accurately before accurate structure factors can be determined. It proved to be very difficult to refine four DW factors simultaneously in one QCBED experiment, especially when structure factors and absorption factors are also relaxed simultaneously. Under these conditions the refinements may easily be trapped in a local minimum instead of the global minimum. To overcome this problem, we used a two-step approach to measure DW factors, in which $B(\mathrm{Fe})_{11}$ and $B(\mathrm{Pd})_{11}$ are obtained first, and $B(\mathrm{Fe})_{33}$ and $B(\mathrm{Pd})_{33}$ later.

For a tetragonal structure, the temperature factor in the structure-factor equation for a particular reflection *hkl* takes the form (Willis & Pryor, 1975)

$$\exp(-Bs^2) = \exp\left[-\frac{1}{4}\left(\frac{h^2+k^2}{a^2}B_{11} + \frac{l^2}{c^2}B_{33}\right)\right]. \qquad (6)$$

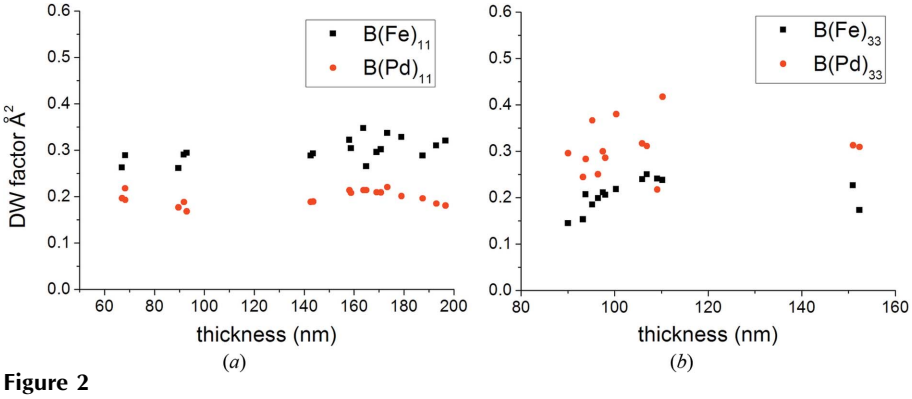

Figure 2
Refined DW factors for Fe and Pd. (*a*) $B(\mathrm{Fe})_{11}$ and $B(\mathrm{Pd})_{11}$ *versus* thickness, (*b*) $B(\mathrm{Fe})_{33}$ and $B(\mathrm{Pd})_{33}$ *versus* thickness.

Along the [001] = [*uvw*] orientation, all the reflections in the zero-order Laue zone (ZOLZ) of the tetragonal crystal have the form of *hk*0 and satisfy $hu + kv + lw = 0$. From equation (6) it follows when *l* is zero, the corresponding temperature factor is not influenced by B_{33}. Structure factors of *hk*0 for $L1_0$ FePd are only influenced by $B(\mathrm{Fe})_{11}$ and $B(\mathrm{Pd})_{11}$, and not by $B(\mathrm{Fe})_{33}$ and $B(\mathrm{Pd})_{33}$. In this case only two different DW factors need to be refined, which greatly simplifies the refinement process.

Off-zone-axis multi-beam condition CBED patterns from different sample thicknesses were acquired from near-[001] orientations. Similar to the case of *B*2-ordered NiAl (Sang *et al.*, 2010*c*), we chose a multi-beam orientation that is sensitive to both DW factors and structure factors. In this condition, 200, 020 and 220 reflections fulfil Bragg's law exactly (Fig. 1*a*). Those three beams are strongly excited and dynamical interactions among them and the transmitted beam make the intensity distribution in those patterns sensitive to DW factors and simultaneously the respective structure factors. The refinement was carried out by relaxation of $B(\mathrm{Fe})_{11}$ and $B(\mathrm{Pd})_{11}$ along with the low-order structure factors 110 and 200. The inclusion of 220 in the refinement was shown to cause large scatter of the resulting DW factors and 220 was therefore not included. Based on convergence criteria, approximately 315 exact beams and 194 Bethe beams were included to ensure that the truncation error caused by an insufficient number of beams is negligible. The resulting values of $B(\mathrm{Fe})_{11}$ and $B(\mathrm{Pd})_{11}$ from CBED patterns acquired at different sample thicknesses are shown in Fig. 2(*a*). The R_{W} values for those refinements are generally lower than 0.15 with some as low as 0.1. Average values for $B(\mathrm{Fe})_{11}$ and $B(\mathrm{Pd})_{11}$ are 0.30 (2) and 0.20 (2) Å^2, respectively. The results presented in Fig. 2(*a*) are very stable. Stable results from different sample thicknesses indicate the reliability of this QCBED method. According to the Bloch-wave formalism, DW and structure factors should be independent of sample thickness. However, owing to sample contamination and other problems, other QCBED methods, like the excited-row QCBED method, have not been capable of obtaining stable DW factors from thick areas (Swaminathan *et al.*, 1993).

CBED patterns in the near-[110] orientation (Fig. 1*b*) were acquired subsequently to obtain $B(\mathrm{Fe})_{33}$ and $B(\mathrm{Pd})_{33}$. This multi-beam condition includes simultaneously excited $1\bar{1}\bar{1}$, 002, $2\bar{2}2$, $2\bar{2}0$ and $1\bar{1}3$ reflections. In the refinement, $B(\mathrm{Fe})_{33}$ and $B(\mathrm{Pd})_{33}$ and six low-order structure factors were relaxed simultaneously while $B(\mathrm{Fe})_{11}$ and $B(\mathrm{Pd})_{11}$ were fixed to the values obtained above. Approximately 286 exact beams and 207 Bethe beams were included to ensure that the truncation error caused by an insufficient number of beams is negligible. Fig. 2(*b*) shows stable $B(\mathrm{Fe})_{33}$ and $B(\mathrm{Pd})_{33}$ values

obtained from different sample thicknesses. The average values for the anisotropic magnitudes $B(\mathrm{Fe})_{33}$ and $B(\mathrm{Pd})_{33}$ are 0.21 (3) and 0.31 (5) Å^2, respectively.

3.2. Structure factors

Electron structure factors are subsequently refined using the experimentally measured DW factors, which are fixed during refinements, as this yields more stable refinement results, *i.e.* the resulting electron structure factors are the same as structure factors obtained with simultaneously refined DW factors; however the scatter is smaller. CBED patterns from four low-index orientations [001], [110], [100] and [101], which can provide low-order structure factors up to 222, were acquired. Off-zone-axis multi-beam orientation patterns for $L1_0$ FePd along different orientations are shown in Fig. 1. Discs which intersect the Ewald sphere are strongly excited and therefore used in the refinement. For patterns in the near-[001] orientation, 200, 020 and 220 reflections are excited. For patterns in the near-[110] orientation, $1\bar{1}\bar{1}$, 002, $2\bar{2}2$, $2\bar{2}0$ and $1\bar{1}3$ reflections are excited. For patterns in the near-[100] orientation, 002, 020 and 022 reflections are excited. For patterns in the near-[101] orientation, $\bar{1}\bar{1}1$, 020, $\bar{2}02$, $\bar{2}22$ and $\bar{1}31$ reflections are excited. Intensity distributions in those patterns are very sensitive to the changes in the structure-factor content of strongly excited reflections. The comparison of experimentally acquired CBED discs with simulated discs after refinements is shown in Fig. 3. Each CBED pattern was refined two times. In the first refinement, structure factors were approximated with IAM values and fixed. In the second refinement, the structure factors were included using IAM values as starting values and relaxed during the refinement. The inclusion and relaxation of structure factors in the refinement improve the quality, reflected in a decrease in R_W values from 0.14, 0.28, 0.39 and 0.20 to 0.11, 0.14, 0.14 and 0.14 for Figs. 1(*a*), 1(*b*), 1(*c*) and 1(*d*), respectively. All the refinements have been greatly improved by relaxing low-order structure factors, indicating that these structure factors are greatly influenced by bonding. Unlike in the excited-row method, where changes in the structure factors mainly cause changes in peak intensity but not in peak position (Spence & Zuo, 1992), here in the off-zone-axis multi-beam conditions the two-dimensional features change significantly if structure factors change, as can be seen clearly in Fig. 3(*c*). The features in the third column in Fig. 3(*c*) show that the IAM approximation fails for $L1_0$ FePd. This beam orientation is capable of detecting minute changes of structure factors. The refined thicknesses are 143.65, 97.32, 146.67 and 78.83 nm for Figs. 1(*a*), 1(*b*), 1(*c*) and 1(*d*), respectively.

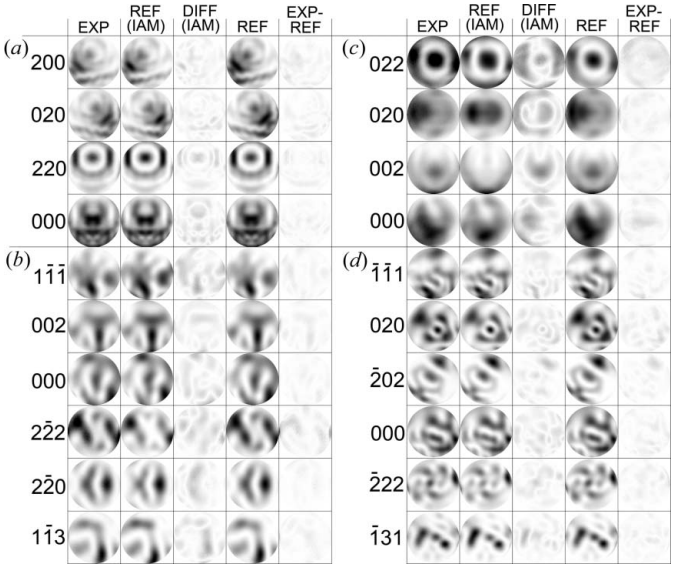

Figure 3
Refinement results of CBED patterns recorded from different orientations. The first column in each part shows experimental discs. The second column shows calculated discs by using obtained DW factors and assuming the IAM. The fourth column shows calculated discs by relaxing structure factors and fixing DW factors. The third column and the fifth column show the absolute value of deviation between column 1 and column 2, and between column 1 and column 4, respectively.

Fig. 4 shows how the experimentally obtained structure factors vary with sample thickness. Both 110 and 200 structure factors are stable over a large sample thickness range.

Electron structure factors are listed in Table 1. X-ray structure factors were converted from electron-diffraction structure factors using the Mott formula (Spence & Zuo, 1992) and measured DW factors. Table 2 shows a comparison of X-ray structure factors with IAM values, which shows that low-order structure factors are within the error significantly different from IAM structure factors. Even some higher-order structure factors, *e.g.* F_{222}, still exhibit significant differences from the IAM approximation, indicating that charge transfer and localization could possibly affect even higher-order structure factors. This effect is graphically illustrated in Fig. 5. The difference between measured electron structure factors and IAM electron structure factors along with standard deviations are plotted in Fig. 5(*a*) for each reflection. Standard deviations are calculated for each structure factor and represented as an error bar. A similar plot for X-ray structure factors is shown in Fig. 5(*b*).

Figs. 5(*a*) and 5(*b*) show that, for low-order reflections, generally the standard deviation is less than the difference between the experimental value and the IAM value (the error

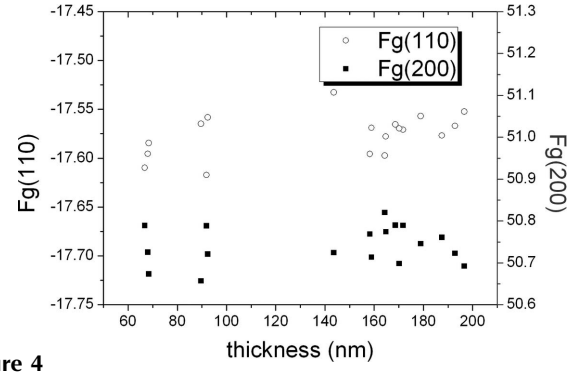

Figure 4
Refined structure factors *versus* thickness for patterns acquired in the near-[001] zone axis [left axis: $F_g(110)$, right axis: $F_g(200)$].

bar does not intersect with the x axis). The standard deviation for electron structure factors is very small for low-order structure factors since the pattern is more sensitive to changes in low-order structure factors than higher-order structure factors. This trend is magnified in X-ray structure factors, because in the Mott formula [equation (2)] used for conversion from electron to X-ray structure factors the scaling factor s^2 is included, which significantly increases the error for high-order reflections. As can be seen from Table 2, the accuracy of structure factors for 001, 110, 111 and 200 is as high as 0.1%, while for the higher-order reflections, such as 113 and 222, the accuracy is reduced to of the order of 1%.

4. Discussion

4.1. Sensitivity to DW factors

Generally, QCBED patterns are not as sensitive to the changes in DW factors as to changes in structure factors. As the determination of DW factors is achieved through refinement of high-order electron structure factors, the sensitivity to changes in DW factors depends on the sensitivity of the CBED pattern to changes in high-order electron structure factors. Since low-order reflections are excited more strongly than high-order reflections, CBED patterns are more sensitive to changes in low-order structure factors than to changes in DW factors. The accuracy in refinements for structure factors can be as high as 0.1%, while for the DW factors the accuracy of the refinements remains always of the order of 10%. For this reason previous efforts to determine DW factors by QCBED remained unsuccessful (Nüchter *et al.*, 1998*a*). It is essential to select an orientation which yields DW factors that are as stable as possible. In the following discussion we assume isotropic DW factors, as the sensitivity of the four independent DW factors cannot be conveniently graphically represented. However, the general trend observed for isotropic DW factors holds true also for anisotropic DW factors (observed in refinement, not shown here). Assuming isotropic DW factors, 19 patterns near [001], 14 patterns near [110], 28 patterns near

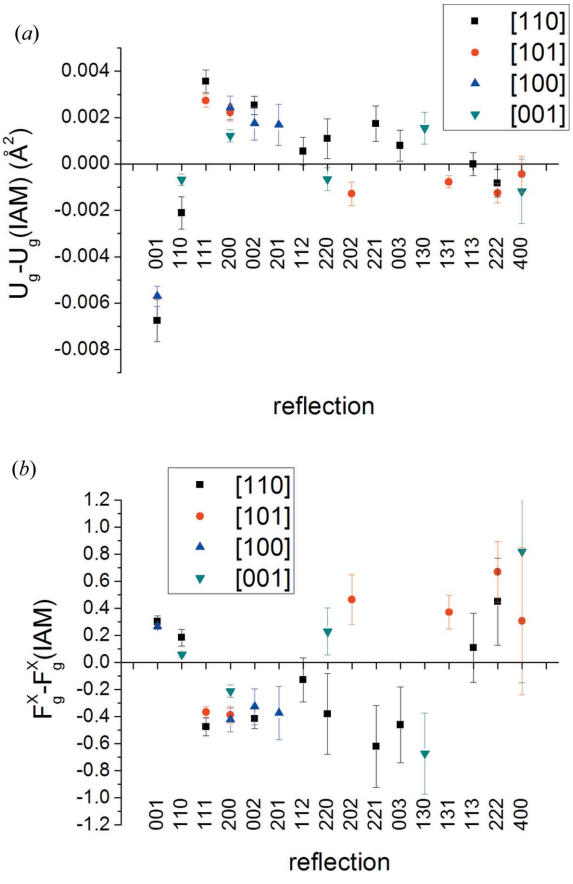

Figure 5
Difference between measured electron structure factors U_g and IAM values U_g(IAM) *versus* reflection g_{hkl} (*a*) and difference between measured X-ray structure factors F_g^X and IAM values F_g^X(IAM) *versus* reflection g_{hkl} (*b*).

Table 1
Electron structure factors U_g (Å^{-2}) of $L1_0$ FePd refined from different zone axes and comparison with IAM values.

Family of **g** contained in the zone $\langle uvw \rangle$	U_g				
	⟨110⟩	⟨101⟩	⟨100⟩	⟨001⟩	IAM
001	−0.0303 (9)		−0.0293 (4)		−0.0236
110	−0.0287 (7)			−0.0273 (2)	−0.0266
111	0.1309 (5)	0.1301 (3)			0.1274
200		0.1164 (4)	0.1166 (5)	0.1154 (3)	0.1141
002	0.1129 (4)		0.1121 (7)		0.1103
201			−0.0210 (9)		−0.0227
112	−0.0196 (6)				−0.0201
220	0.0815 (9)			0.0797 (5)	0.0804
202		0.0772 (5)			0.0785
221	−0.0151 (8)				−0.0169
003	−0.0144 (7)				−0.0152
130				−0.0145 (7)	−0.0160
131		0.0650 (3)			0.0657
113	0.0632 (5)				0.0632
222	0.0604 (6)	0.0599 (4)			0.0612
400		0.0504 (8)		0.0496 (14)	0.0508

Table 2
X-ray structure factors F_g^X of $L1_0$ FePd refined from different zone axes and comparison with IAM values.

Family of **g** contained in the zone $\langle uvw \rangle$	F_g^X				
	⟨110⟩	⟨101⟩	⟨100⟩	⟨001⟩	IAM
001	−18.44 (4)		−18.47 (2)		−18.738
110	−17.45 (6)			−17.58 (2)	−17.634
111	53.53 (7)	53.64 (4)			54.006
200		50.56 (6)	50.53 (9)	50.74 (5)	50.951
002	49.51 (7)		49.6 (1)		49.929
201			−15.1 (2)		−14.732
112	−13.93 (16)				−13.803
220	41.3 (3)			41.9 (2)	41.705
202		41.5 (2)			41.078
221	−13.6 (3)				−12.980
003	−12.7 (3)				−12.226
130				−13.5 (3)	−12.787
131		37.5 (1)			37.110
113	36.3 (3)				36.172
222	36.0 (3)	36.2 (2)			35.578
400		32.4 (5)		32.9 (9)	32.128

Table 3
Refined isotropic DW factors using patterns along different orientations.

	⟨001⟩		⟨110⟩		⟨100⟩		⟨101⟩	
	$B(\mathrm{Fe})_{\mathrm{iso}}$	$B(\mathrm{Pd})_{\mathrm{iso}}$	$B(\mathrm{Fe})_{\mathrm{iso}}$	$B(\mathrm{Pd})_{\mathrm{iso}}$	$B(\mathrm{Fe})_{\mathrm{iso}}$	$B(\mathrm{Pd})_{\mathrm{iso}}$	$B(\mathrm{Fe})_{\mathrm{iso}}$	$B(\mathrm{Pd})_{\mathrm{iso}}$
Value (Å^2)	0.30	0.20	0.23	0.25	0.22	0.27	0.11	0.36
Standard deviation (Å^2)	0.02	0.02	0.03	0.04	0.16	0.08	0.16	0.14

[100] and 12 patterns near [101] were refined relaxing isotropic DW factors and several low-order structure factors simultaneously. The resulting DW factors $B(\mathrm{Fe})_{\mathrm{iso}}$, $B(\mathrm{Pd})_{\mathrm{iso}}$ and corresponding standard deviations are listed in Table 3. The values for the isotropic DW factors $B(\mathrm{Fe})_{\mathrm{iso}}$ and $B(\mathrm{Pd})_{\mathrm{iso}}$ should fall in the range limited by the anisotropic DW factors for the respective elements in the $L1_0$-ordered structure. The values for $B(\mathrm{Fe})_{\mathrm{iso}}$ and $B(\mathrm{Pd})_{\mathrm{iso}}$ determined from orientations near the [001] zone axis are of high accuracy as can be seen from Table 3. The equivalent DW factors refined from patterns near the [110] zone axis are also stable. The isotropic DW factor $B(\mathrm{Fe})_{\mathrm{iso}}$ was determined as 0.23 (3) Å^2, which lies in the range of $B(\mathrm{Fe})_{11}$ = 0.30 (2) Å^2 and $B(\mathrm{Fe})_{33}$ = 0.21 (3) Å^2, and $B(\mathrm{Pd})_{\mathrm{iso}}$ was determined as 0.25 (4) Å^2, which lies between $B(\mathrm{Pd})_{11}$ = 0.20 (2) Å^2 and $B(\mathrm{Pd})_{33}$ = 0.31 (5) Å^2.

DW factors refined from the other two orientations [100] and [101] are not very stable. In the case of the near-[101] orientation the standard deviation is as high as 160%. Results in Table 3 are visualized in the graphs in Fig. 6, which plot contour lines of R_{W} as the isotropic DW factors $B(\mathrm{Fe})_{\mathrm{iso}}$ and $B(\mathrm{Pd})_{\mathrm{iso}}$ are varied. In contour maps derived from refinements of CBED data from near-[001] and [110] orientations, unique global minima, surrounded by near-circular contour lines, can be observed. In the contour map from near [101], no global minimum can be observed. Instead two equally good R_{W} valleys occur, which means that no unique set of $B(\mathrm{Fe})_{\mathrm{iso}}$ and $B(\mathrm{Pd})_{\mathrm{iso}}$ can be obtained from near-[101] orientations. The refinement of near-[101] orientation yields two sets of $B(\mathrm{Fe})_{\mathrm{iso}}$ and $B(\mathrm{Pd})_{\mathrm{iso}}$, which are equally likely (this was also observed in refinements using anisotropic DW factors). The contour map for the near-[100] orientation shows irregular contour lines. However, while $B(\mathrm{Pd})_{\mathrm{iso}}$ is reasonably well determined for this later orientation, the global minimum extends parallel to the $B(\mathrm{Fe})_{\mathrm{iso}}$ axis, which reflects a large uncertainty for values of $B(\mathrm{Fe})_{\mathrm{iso}}$. Since the patterns obtained from near-[001] and [110] zone axes are more sensitive to changes in DW

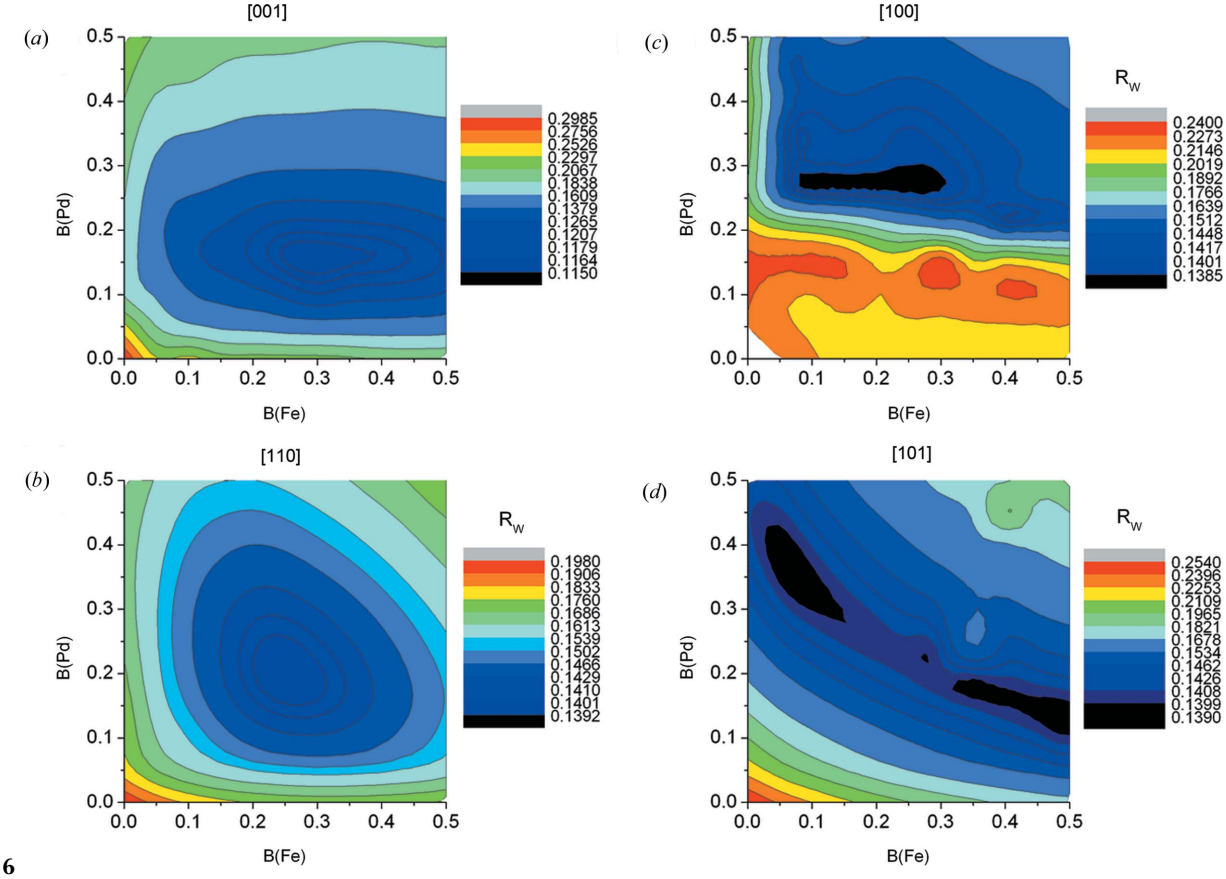

Figure 6
Contour maps of R_{W} with changing assumed isotropic DW factors along zone axes (*a*) [001], (*b*) [110], (*c*) [100] and (*d*) [101].

factors and refinements always result in a global minimum in the contour map, we used these two orientations to obtain anisotropic DW factors.

High-order structure factors can be relatively accurately approximated using IAM values. Low-order structure factors are strongly affected by bonding effects, which cause significant deviations from IAM approximations. Hence, it might be concluded that the use of high-index zone-axis orientations is favorable as low-order structure factors can be avoided in the refinement. However, Fig. 6 and Table 3 tell us that high-index zone-axis CBED patterns are not necessarily a good choice since they are not sufficiently sensitive to refine DW factors. To obtain accurate DW factors, near-low-index zone-axis CBED patterns offer a better choice with improved sensitivity regarding changes in DW factor. We speculate that here the increased number of strongly excited beams and the consequently enhanced dynamic beam interactions are associated with the improved sensitivity of the near-zone-axis patterns regarding DW factor changes.

4.2. Sensitivity to structure factors

We refined CBED patterns, varying the number of relaxed low-order structure factors, to demonstrate the sensitivity of the intensity distribution in an off-zone-axis multi-beam condition pattern with changes in structure factors. As shown in Fig. 7(*a*), the first value R_W = 0.144 was obtained using measured DW factors from §3.1 and approximating all the structure factors to IAM values. The next value in the plot, R_W = 0.136, was obtained using measured DW factors and relaxing only the 110 structure factor. All other structure factors were fixed to the IAM values. Analogously, R_W = 0.116 was obtained by relaxing the 110 and 200 structure factors. Each time an additional structure factor was included and relaxed in the refinement. As can be seen from Fig. 7, R_W values initially decrease dramatically as the first few low-order structure factors are relaxed, and finally become constant. R_W values improve as more structure factors are relaxed. Low-order structure factors are affected by charge transfer and localization, and therefore deviate significantly from IAM values. Hence refinements that use fixed IAM values naturally yield higher R_W values. As more structure factors with increasing order are relaxed, R_W values decrease monotonically until a minimum is obtained. This can be attributed to the fact that the pattern intensity is not sensitive to the next higher-order structure factor or that the IAM approximation describes sufficiently well these higher-order structure factors. Intensity distributions in off-zone-axis multi-beam conditions are very sensitive to changes of a few low-order structure factors. However, there is a limit after which off-zone-axis multi-beam patterns are not significantly influenced by high-order structure factors. Surprisingly, although the patterns are less sensitive to higher-order structure factors, the refined results (Fig. 5*a*) show that standard deviations of electron structure factors do not significantly increase from low-order to high-order structure factors. The high scatter shown in Fig. 5(*b*) for high-order X-ray structure factors is caused by the term s^2 in the Mott formula [equation (4)], as discussed in §3.2.

Fig. 7 also shows that this multi-beam method can be very sensitive to slight changes of structure factors, which has been shown for silicon (Sang *et al.*, 2010*b*) and *B*2 NiAl (Sang *et al.*, 2010*c*). Under exactly the same off-zone-axis multi-beam condition, the change of R_W value due to relaxation of more structure factors along the same zone axis [001] can be reduced from 0.36 to 0.14 for NiAl and from 0.14 to 0.11 for $L1_0$ FePd, which shows that for FePd low-order structure factors deviate less from IAM values than is the case for NiAl and that FePd has a smaller (relative and/or total) amount of charge transfer and localization than NiAl. Thus, the measurements of structure factors for the case of FePd require higher precision than for NiAl in order to become sensitive to effects from interatomic bonding.

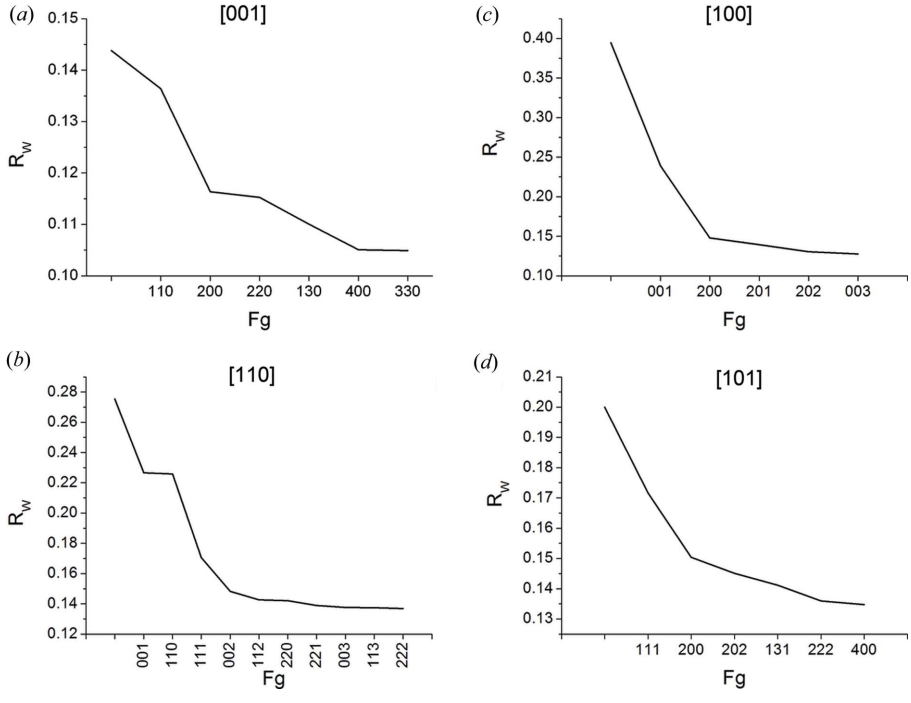

Figure 7
Changes of R_W as increasing numbers of reflections are included and relaxed in the refinement for patterns taken along zone axes (*a*) [001], (*b*) [110], (*c*) [100] and (*d*) [101].

Fig. 8(*a*) shows a comparison of the electron density along the ⟨101⟩ orientation of the *tP*4 unit cell, which is equivalent to the ⟨111⟩ orientation of the *tP*2 unit cell of $L1_0$-ordered γ_1-FePd. The IAM electron density was obtained by Fourier transformation of IAM X-ray structure factors satisfying $h^2 + k^2 + l^2 < 900$, which is sufficient based on a convergence test. For the calculation of the experimental electron

density, for low-order X-ray structure factors up to 311 measured values were used in the Fourier transformation instead of IAM values. While from Fig. 8(*a*) virtually no difference between the IAM model approximation and the experimentally determined charge-density distribution is discernible, plotting the difference between the IAM approximation and the experimentally determined charge density (Fig. 8*b*) shows some small changes. In both plots of Fig. 8, the abscissa (*x* axis) ranges from 0.0 to 1.0, with corresponding positions of the Fe atoms at 0.0 and 1.0 and the position of the Pd atom at 0.5. This indicates that some charge is transferred from the Fe atoms both to the Pd atom and to locations between the Fe and the Pd atoms. This result not only shows that our technique is accurate enough to detect changes as small as 0.01% of the total signal, but that our experimentally determined structure and DW factor data are also, in principle, accurate enough to construct charge-difference maps. Why we refrain here from presenting an actual charge-difference map will be explained in the next section.

4.3. Self-consistency of structure factors refined from different zone axes

Absolute structure-factor values have to be the same no matter from which near-zone-axis orientation they have been obtained. Our structure-factor refinements from different near-zone-axis orientations show good correspondence and

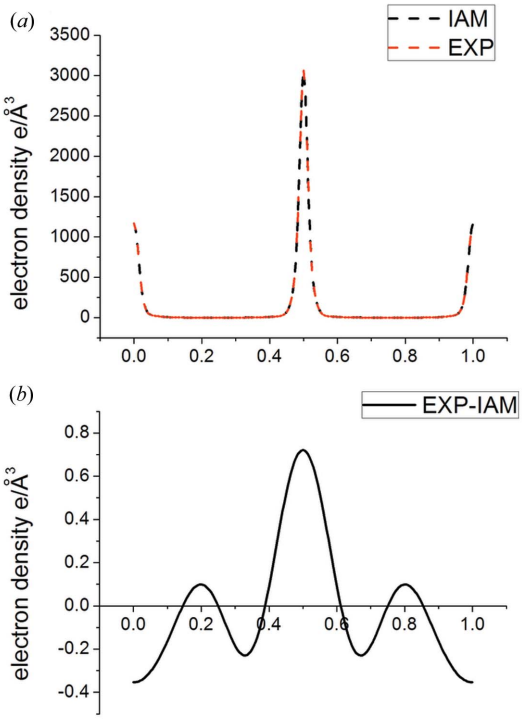

Figure 8
(*a*) Comparison of the electron density obtained by the IAM model approximation and the experimental CBED measurements along the ⟨101⟩ orientation in the *tP*4 unit cell, which is equivalent to the ⟨111⟩ orientation of the *tP*2 unit cell. (*b*) Difference of the electron density from the IAM approximation and the experimentally determined structure factors along the same direction.

are self-consistent data sets, as can be seen from Fig. 5. The same structure factor obtained from different orientations is, with the exception of the structure factor 220, always consistently larger or smaller than the IAM value. When the 220 reflection is refined from the near-[001] zone axis, the X-ray structure factor is larger than the IAM value. Refinement from the near-[110] zone-axis orientation yields a 220 X-ray structure factor smaller than the IAM value.

This inconsistency is possibly caused by the insensitivity of those two orientations to changes of the 220 reflection. As can be seen in Figs. 7(*a*) and 7(*b*), the relaxation of the 220 reflection results in only a very minor decrease of the respective R_W value. The other possible reason might be that the zero-background assumption might not be applicable here (Nakashima & Muddle, 2010). An alternative background-correction method is under investigation (Nakashima & Muddle, 2010). A third reason could be related to the ferromagnetic nature of $L1_0$ FePd with its high symmetry and unique easy magnetization *c* axis. The interaction between the incident electrons and magnetic field within the crystal is different for different zone axes. For the non-magnetic, isostructural intermetallic phase $L1_0$ TiAl, structure factors obtained with the off-axis CBED method from different zone axes agree very well (unpublished data). We probed the hypothesis that the ferromagnetism may have effects on the structure-factor determination by CBED for $L1_0$ FePd by comparing electron structure factors $U_g(110)$ and $U_g(200)$ obtained from different zone axes.

Aside from the data presented above in Tables 1 and 2, we obtained additional structure-factor measurements using off-zone-axis multi-beam conditions near two other zone axes, namely [112] and [332]. Data for the two electron structure factors $U_g(110)$ and $U_g(200)$ from different zone axes are compiled in Fig. 9, where the *x* axis is the sine or cosine of the angle θ, the misorientation angle between the zone-axis orientation of the sample for which the electron structure factor was obtained by the off-zone-axis multi-beam CBED method and the easy magnetization axis [001] of the $L1_0$ FePd phase. Both structure factors exhibit linear relationships with respect to the respective trigonometric function of the angle between the incident electron beam, [*uvw*], and the easy magnetization axis, [001]. We speculate that this systematic change of refined structure factor is related to the angular dependence of the interaction of the magnetic field of $L1_0$-ordered FePd and the incident fast electrons used for CBED. The conventional Bloch-wave formalism does not include magnetic field terms (Bethe, 1928). The treatment of Bloch electrons in a uniform magnetic field has been investigated before (Blount, 1962; Fischbeck, 1970; Brown, 1964). Shen & Laughlin (1990) reported that only the magnetic fields parallel to the incident beam would not influence the intensity of CBED patterns. Therefore, only structure factors from the near-[001] zone axis (*i.e.* U_{110}, U_{200}, U_{220}, U_{130} and U_{400}) are not influenced by the magnetic field and do not have to be corrected. All structure factors (U_{001}, U_{111}, U_{002}, U_{201}, U_{202}, U_{311}, U_{222} *etc.*) that cannot be determined from the [001] zone axis have to be obtained from other near-zone-axis

orientations and need to be corrected. Currently the adaptation of interaction between the fast electron and the magnetic field in the Bloch-wave formalism is not readily available. Reasonable electron charge-density maps cannot be constructed without inclusion of the structure factors that cannot be obtained from the near-[001] zone-axis orientation, *i.e.* without U_{hkl} with $l \neq 0$. Therefore, we do not present a charge-density map here. Further investigation on how to correct those structure factors and construction of a charge-density map is in progress.

4.4. Advantage of using multi-beam off-zone-axis condition

The multi-beam near-zone-axis CBED method proposed by Sang *et al.* (2010*a*,*b*,*c*) for the simultaneous refinements of precise Debye–Waller factors and structure factors was successfully tested on silicon and NiAl. Here, we applied this method to measure DW factors and structure factors of a ferromagnetic chemically ordered transition-metal-based intermetallic phase with tetragonal symmetry that has not been investigated with QCBED before. The challenge of the investigation of $L1_0$-ordered FePd lies in the tetragonality of its structure and the relatively small charge transfer leading to a very limited magnitude of the intermetallic bonding related charge localization. The simultaneous determination of DW factors and structure factors requires careful selection of beam orientations and a thorough refinement procedure. Off-zone-axis multi-beam conditions proved to be sufficiently precise and accurate to yield high-quality structure and DW factors. Anisotropic DW factors were obtained subsequently from conditions which yield distinct global minima (Fig. 6). Structure factors were measured from patterns that are sufficiently sensitive to changes in structure-factor content (Fig. 7). The sensitivity results from mutual interactions among the excited diffracted beams and with the transmitted beam. The accuracy for the FePd results is not as high as in the case of NiAl, because in FePd the bonding-induced charge transfer and localization is much smaller in magnitude.

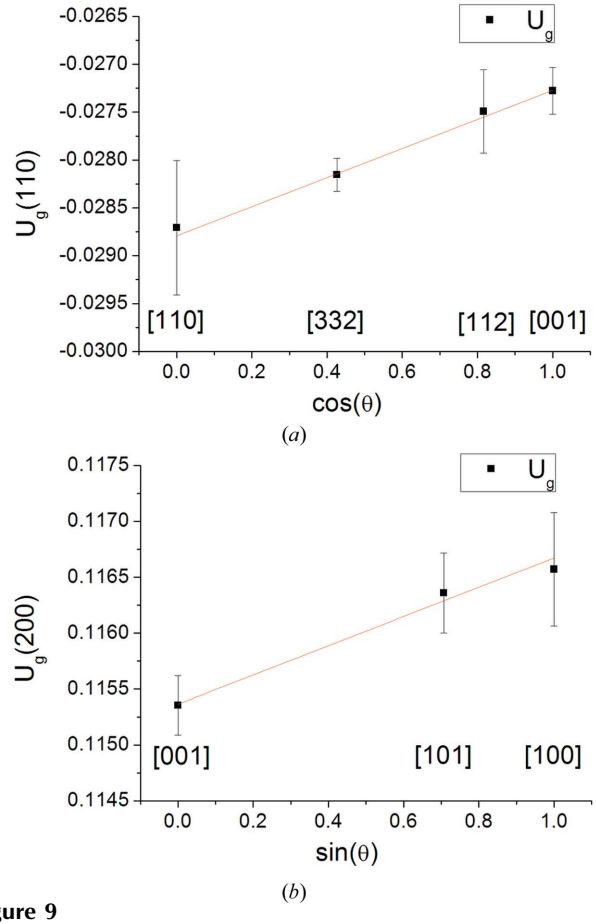

Figure 9
Dependence of the electron structure factors (*a*) $U_g(110)$ on $\cos(\theta)$ and (*b*) $U_g(200)$ on $\sin(\theta)$, where θ is the angle between the zone-axis orientation, [*uvw*], used for CBED from which the structure factor was refined and the easy magnetization axis [001] of the $L1_0$ FePd phase.

5. Conclusion

Highly accurate structure factors and anisotropic DW factors for $L1_0$-ordered FePd were simultaneously measured using a multi-beam near-zone-axis CBED method. $B(\mathrm{Fe})_{11}$, $B(\mathrm{Fe})_{33}$, $B(\mathrm{Pd})_{11}$, $B(\mathrm{Pd})_{33}$ are 0.30 (2), 0.21 (3), 0.20 (2) and 0.31 (5) Å^2, respectively. Low-order electron diffraction and X-ray diffraction structure factors up to 222 were measured. Several low-order structure factors have an accuracy higher than 0.1%. Additionally, we detected an influence of the magnetic field of the $L1_0$-ordered γ_1-FePd on the intensity distribution in CBED patterns. Depending on the orientation of the magnetic field of the investigated sample area with the incident beam, the influence on the intensity distribution and the ensuing change in structure factor can be more or less severe. At this moment there is no appropriate treatment of the interaction of magnetic fields with fast electrons in the Bloch-wave formalism used in refinements for structure-factor determination. For the first time the multi-beam off-axis CBED method was used to obtain large sets of structure factors for a chemically ordered binary intermetallic transition-metal compound with a small unit cell of tetragonal symmetry. This method has been proven to yield highly accurate and precise structure and DW factors, and offers potential for further application.

This work was supported by a grant of the Office of Basic Energy Sciences, Division of Materials Science and Engineering, of the US DOE (grant No DE-FG02-08ER46545). Additional support has been received from the National Science Foundation through access to the TeraGrid resources provided by TACC under grant No. TG-DMR100102 and the Center for Molecular and Materials Simulations at the University of Pittsburgh.

References

Al-Ghaferi, A., Muellner, P., Heinrich, H., Kostorz, G. & Wiezorek, J. M. K. (2006). *Acta Mater.* **54**, 881–889.
Bethe, H. (1928). *Ann. Phys. Berlin*, **392**, 55–129.
Bird, D. M. & King, Q. A. (1990). *Acta Cryst.* A**46**, 202–208.
Blount, E. I. (1962). *Phys. Rev.* **126**, 1636.

Brown, E. (1964). *Phys. Rev. A*, **133**, 1038.
Butt, N. M., Bashir, J., Willis, B. T. M. & Heger, G. (1988). *Acta Cryst.* A**44**, 396–399.
Buxton, B. F., Eades, J. A., Steeds, J. W. & Rackham, G. M. (1976). *Philos. Trans. R. Soc. London Ser. A*, **281**, 171–194.
Doyle, P. A. & Turner, P. S. (1968). *Acta Cryst.* A**24**, 390–397.
Fischbeck, H. J. (1970). *Phys. Status Solidi B*, **38**, 11–62.
Friis, J., Jiang, B., Marthinsen, K. & Holmestad, R. (2005). *Acta Cryst.* A**61**, 223–230.
Friis, J., Jiang, B., Spence, J., Marthinsen, K. & Holmestad, R. (2004). *Acta Cryst.* A**60**, 402–408.
Georgopoulos, P. & Cohen, J. B. (1977). *Scr. Metall.* **11**, 147–150.
Holmestad, R. & Birkeland, C. R. (1998). *Philos. Mag. A*, **77**, 1231–1254.
Ichitsubo, T. & Tanaka, K. (2004). *J. Appl. Phys.* **96**, 6220–6223.
Jiang, B., Friis, J., Holmestad, R., Zuo, J. M., O'Keeffe, M. & Spence, J. C. H. (2004). *Phys. Rev. B*, **69**, 245110.
Jiang, B., Zuo, J. M., Jiang, N., O'Keeffe, M. & Spence, J. C. H. (2003). *Acta Cryst.* A**59**, 341–350.
Nakashima, P. N. H. & Muddle, B. C. (2010). *Phys. Rev. B*, **81**, 115135.
Nüchter, W., Weickenmeier, A. L. & Mayer, J. (1998*a*). *Acta Cryst.* A**54**, 147–157.
Nüchter, W., Weickenmeier, A. L. & Mayer, J. (1998*b*). *Phys. Status Solidi A*, **166**, 367–379.
Ogata, Y., Tsuda, K., Akishige, Y. & Tanaka, M. (2004). *Acta Cryst.* A**60**, 525–531.
Sang, X., Kulovits, A. & Wiezorek, J. M. K. (2010*a*). *Microsc. Microanal.* **16** (Suppl. 2), 938–939.
Sang, X. H., Kulovits, A. & Wiezorek, J. M. K. (2010*b*). *Acta Cryst.* A**66**, 685–693.
Sang, X. H., Kulovits, A. & Wiezorek, J. M. K. (2010*c*). *Acta Cryst.* A**66**, 694–702.
Saunders, M., Bird, D. M., Zaluzec, N. J., Burgess, W. G., Preston, A. R. & Humphreys, C. J. (1995). *Ultramicroscopy*, **60**, 311–323.
Saunders, M., Fox, A. G. & Midgley, P. A. (1999). *Acta Cryst.* A**55**, 480–488.
Shen, Y. & Laughlin, D. E. (1990). *Philos. Mag. Lett.* **62**, 187–193.
Spence, J. C. H. (1993). *Acta Cryst.* A**49**, 231–260.
Spence, J. C. H. & Zuo, J. M. (1992). *Electron Microdiffraction.* New York: Plenum Press.
Streltsov, V. A., Nakashima, P. N. H. & Johnson, A. W. S. (2001). *J. Phys. Chem. Solids*, **62**, 2109–2117.
Swaminathan, S., Jones, I. P., Zaluzec, N. J., Maher, D. M. & Fraser, H. L. (1993). *Mater. Sci. Eng. A*, **170**, 227–235.
Tsuda, K. & Tanaka, M. (1995). *Acta Cryst.* A**51**, 7–19.
Willis, B. T. M. & Pryor, A. W. (1975). *Thermal Vibrations in Crystallography*. London: Cambridge University Press.
Zhu, J., Miao, Y. & Guo, J. T. (1997). *Acta Mater.* **45**, 1989–1994.
Zuo, J. M. (1992). *Ultramicroscopy*, **41**, 211–223.
Zuo, J. M., Kim, M., O'Keeffe, M. & Spence, J. C. H. (1999). *Nature (London)*, **401**, 49–52.
Zuo, J. M., O'Keeffe, M., Rez, P. & Spence, J. C. H. (1997). *Phys. Rev. Lett.* **78**, 4777–4780.